Nanostructures

DOI: 10.1002/anie.201403842

Self-Supported Cu_3P Nanowire Arrays as an Integrated High-Performance Three-Dimensional Cathode for Generating Hydrogen from Water**

*Jingqi Tian, Qian Liu, Ningyan Cheng, Abdullah M. Asiri, and Xuping Sun**

Abstract: *Searching for inexpensive hydrogen evolution reaction (HER) electrocatalysts with high activity has attracted considerable research interest in the past years. Reported herein is the topotactic fabrication of self-supported Cu_3P nanowire arrays on commercial porous copper foam (Cu_3P NW/CF) from its $Cu(OH)_2$ NW/CF precursor by a low-temperature phosphidation reaction. Remarkably, as an integrated three-dimensional hydrogen-evolving cathode operating in acidic electrolytes, Cu_3P NW/CF maintains its activity for at least 25 hours and exhibits an onset overpotential of 62 mV, a Tafel slope of 67 mV dec^{-1}, and a Faradaic efficiency close to 100 %. Catalytic current density can approach 10 mA cm^{-2} at an overpotential of 143 mV.*

Hydrogen has been proposed as the principal energy carrier in the hydrogen-economy paradigm.[1] Its widespread use can reduce our dependence on fossil fuels and benefit the environment by reducing greenhouse gas emissions. Electrolysis of water is a simple and promising method for hydrogen production. Usually, efficient electrocatalysts for the hydrogen evolution reaction (HER) are required to achieve high current density at low overpotential. Although platinum-group metals are currently the state-of-the-art hydrogen-evolving catalysts,[2] the scarcity and high cost of platinum limit their wide use.[3] The strongly acidic conditions in proton-exchange membrane (PEM) technology need acid-stable catalysts for PEM-based electrolysis units.[4] Abundant nickel-based alloys are commercially used as HER catalysts, but they are not stable enough to operate in acidic environments.[5] These limitations have motivated significant research efforts to develop acid-stable nonprecious-metal HER catalysts, and significant progress has been indeed made toward this goal in the past years. Molybdenum- and tungsten-based compounds are an exciting family of such catalysts with great success, including MoS_2, $MoSe_2$, Mo_2C, MoB, $NiMoN_x$, $Co_{0.6}Mo_{1.4}N_2$, and WS_2, etc.[6]

Transition-metal phosphides (TMPs) are an important class of compounds with metalloid characteristics and good electrical conductivity,[7] and have been intensively studied for the application as catalysts for the hydrodesulfurization (HDS) reaction.[7,8] Because HDS and the HER work in the same way, in that they both rely on the reversible binding of the catalyst and hydrogen, with hydrogen dissociation to yield H_2S in HDS and with protons bound to the catalyst to promote hydrogen formation in a HER,[9] it is deduced that TMPs may be active for the HER. Recent research, indeed, has proven Ni_2P, FeP, CoP, and MoP to be efficient hydrogen-evolving catalysts.[10]

For electrochemical measurements and practical applications, one has to use polymer binder (nafion or PTFE) to immobilize the catalysts of interest on electrode surfaces. The whole process, however, is time-consuming and the polymer binder may block active sites and inhibit diffusion, thus leading to reduced effective catalytic activity.[11] This problem can be solved by designing binder-free hydrogen-evolving cathodes where the active phases are directly grown on current-collecting substrates. Specifically, self-supported arrays of one-dimensional (1D) nanostructures on current collectors is particularly interesting owing to their vectorial electron-transport property.[12] Indeed, Chen et al. have recently demonstrated the conformal coating of MoS_2 on MoO_3 nanowires directly attached to a fluorine-doped tin oxide conductive substrate, and when used as a HER cathode, this integrated structure shows excellent catalytic activity and stability.[13]

Herein, we report on our recent efforts in developing a novel self-supported Cu_3P nanowire arrays on porous copper foam (Cu_3P NW/CF) by topotactic conversion from its $Cu(OH)_2$ NW/CF precursor. The $Cu(OH)_2$ NW arrays were directly grown on commercial CF by a room-temperature, wet-chemical route first, with a subsequent low-temperature phosphidation reaction (see the Experimental Section for details). As an integrated three-dimensional (3D) cathode for generating hydrogen from acidic water, the Cu_3P NW/CF maintains its activity for at least 25 hours and shows an onset overpotential (η) of 62 mV, a Tafel slope of 67 mV dec^{-1}, and nearly 100 % Faradaic efficiency (FE). An overpotential of 143 mV is needed to afford a catalytic current density of 10 mA cm^{-2}. Both the Cu center (δ^+) and the proximal pendant base P (δ^-) are believed to be responsible for the hydrogen evolution.

[*] Dr. J. Tian, Q. Liu, N. Cheng, Prof. X. Sun
State Key Laboratory of Electroanalytical Chemistry
Changchun Institute of Applied Chemistry
Changchun 130022, Jilin (China)
E-mail: sunxp@ciac.ac.cn
Dr. J. Tian, N. Cheng
Graduate School of the Chinese Academy of Sciences
Beijing 100039 (China)
Prof. A. M. Asiri, Prof. X. Sun
Chemistry Department & Center of Excellence for Advanced Materials Research, King Abdulaziz University
Jeddah 21589 (Saudi Arabia)

[**] This work was supported by the National Natural Science Foundation of China (No. 21175129) and the National Basic Research Program of China (No. 2011CB935800).

Supporting information for this article is available on the WWW under http://dx.doi.org/10.1002/anie.201403842.

The CF changes in color from reddish brown to blue after surface oxidation by ammonium peroxodisulfate (APS) under alkaline conditions with a subsequent color change to black after phosphidiation treatment at 250 °C (see Figure S1 a in the Supporting Information). Figure 1 a shows the X-ray

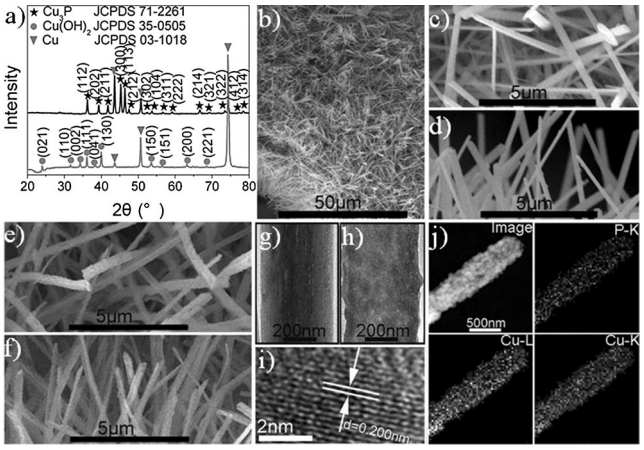

Figure 1. a) XRD patterns of $Cu(OH)_2$ NW/CF and Cu_3P NW/CF. Top-view low- (b) and high-magnification (c) SEM images of $Cu(OH)_2$ NW/CF. d) Side-view high-magnification SEM image of $Cu(OH)_2$ NW/CF. Top-view (e) and side-view (f) high-magnification SEM images of Cu_3P NW/CF. TEM images of $Cu(OH)_2$ (g) and Cu_3P (h) nanowires. i) HRTEM image of Cu_3P nanowire. j) STEM image and the corresponding EDX elemental mapping images of P and Cu for Cu_3P nanowire.

diffraction (XRD) patterns of the precursor on CF before (bottom curve) and after (top curve) phosphidiation. The precursor shows diffraction peaks characteristic of $Cu(OH)_2$ (JCPDS No. 35-0505).[14] In contrast, only peaks corresponding to Cu_3P can be observed for the resulting copper phosphide (JCPDS No. 71-2261).[15] The strong peaks at 43.4°, 50.6°, and 74.6° originate from to the CF substrate (JCPDS No. 03-1018).

Figure 1 b shows the top-view low-magnification scanning electron microscopy (SEM) image of $Cu(OH)_2$ on CF, thus showing that the entire surface of the CF is covered uniformly by a densely packed $Cu(OH)_2$ nanowires (Figure S1 b). A close view of such nanowires (Figure 1 c,d) reveal they extend vertically from the CF with diameters of about 300–400 nm and lengths of up to several micrometers. These observations suggest the formation of $Cu(OH)_2$ nanowire arrays supported on CF. Hou et al. have reported that oxidation of copper foil by APS under alkaline conditions generates aligned $Cu(OH)_2$ nanoribbons and concluded that the interactional stress in the layers of distorted $Cu(OH)_6$ octahedra urges the lamellar sheets to form $Cu(OH)_2$ nanoribbons.[16] The formation of $Cu(OH)_2$ NWs on CF in our present study may adopt a similar growth mechanism.

After phosphidation, the 1D morphology is still preserved (Figure 1 e,f). The corresponding energy dispersive X-ray (EDX) spectrum (see Figure S2 in the Supporting Information) verifies the 3:1 atomic ratio between Cu and P. Figures 1 g,h present the transmission electron microscopy (TEM) images of one single $Cu(OH)_2$ and Cu_3P nanowire, respectively, thus showing the smooth surface of $Cu(OH)_2$ becomes rough after phosphidation. The high-resolution TEM (HRTEM) image taken from the Cu_3P nanowire (Figure 1 i) shows well-resolved lattice fringes with an interplanar distance of 0.200 nm corresponding to the (300) plane of Cu_3P.[15] The scanning TEM (STEM) image and the corresponding EDX elemental mapping images of P and Cu for Cu_3P nanowire are shown in Figure 1 j, further revealing that both P and Cu elements are uniformly distributed in the whole nanowire. All these results clearly confirm the successful topotactic synthesis of Cu_3P NWs/CF by low-temperature phosphidation of its $Cu(OH)_2$ NW/CF precursor. The topotactic conversion of $Cu(OH)_2$ NWs into Cu_3P NWs could be explained as follows: the $Cu(OH)_2$ NWs are reduced to Cu NWs by PH_3, generated in situ from thermally decomposed NaH_2PO_2,[17] and the resulting Cu subsequently catalyzes the decomposition of PH_3 into elemental P, which further reacts with Cu NWs to form Cu_3P NWs.[18] It is important to mention that the phosphidation of CF leads to Cu_3P-microparticle-coated CF (Cu_3P MPs/CF), as shown in Figure S3 of the Supporting Information. Also note that the skeletal structure of the CF was maintained completely throughout the fabrication process, thus enabling its direct use as an integrated 3D cathode for generating hydrogen from water.

Figure 2 a shows the polarization curve of Cu_3P NW/CF (Cu_3P loading: 15.2 mg cm^{-2}) in 0.5 M H_2SO_4 with a scan rate of 2 mV s^{-1}. Blank CF and Cu_3P MP/CF (Cu_3P loading: 15.3 mg cm^{-2}) were also examined for comparison. Blank CF shows poor HER activity with an onset overpotential (η) of 310 mV. In sharp contrast, Cu_3P NW/CF is significantly active for the HER with an onset overpotential as low as 62 mV, and additional negative potential leads to rapid rise of the cathodic current. Note that Cu_3P MP/CF also functions as a hydrogen-evolving cathode but with a much larger onset overpotential (190 mV). The Tafel slope is about 67 and 96 mV/dec for Cu_3P NW/CF and Cu_3P MP/CF, respectively (Figure 2 b). The Tafel slope for commercial 20 % Pt/C was measured to be about 30 mV dec^{-1}, and is consistent with a previous report.[10a] These results suggest superior catalytic activity of Cu_3P NW/CF over Cu_3P MP/CF. The Tafel slopes for Cu_3P-integrated electrodes reveal the HER proceeds by a Volmer–Heyrovsky mechanism.[19] In addition, Cu_3P NW/CF needs overpotentials of 79, 143, and 276 mV to achieve current densities of 1, 10, and 100 mA cm^{-2}, respectively. These values compare favorably to most of reported values for nonplatinum HER catalysts in acidic aqueous electrolytes (see Table S1 in the Supporting Information).

By using the extrapolation method on the Tafel plots (see Figure S4 in the Supporting Information), the exchange current density (j_0) of Cu_3P NW/CF is calculated to be ~0.18 mA cm^{-2}, which is 4.5 times that of Cu_3P MP/CF (~0.04 mA cm^{-2}). The exchange current density is usually expressed in terms of projected or geometric surface area and depends on the surface roughness. The electrochemical surface area can be used as an approximate guide for surface roughness within an order-of-magnitude accuracy.[20] To estimate the effective surface areas of Cu_3P NW/CF and Cu_3P MP/CF, we measured the capacitances of the double layer at the solid/liquid interface of both electrodes.[21] The cyclic voltammograms (CVs) were collected in the region of

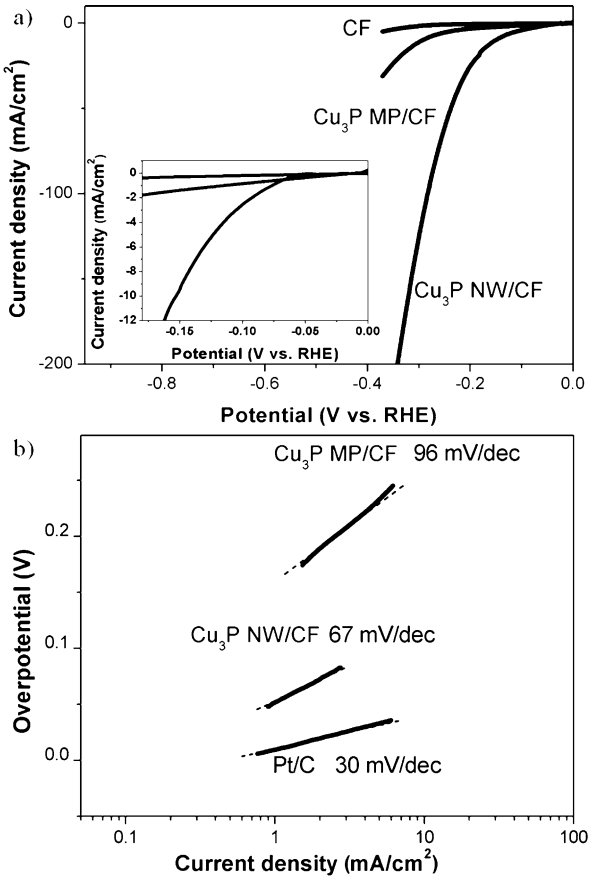

Figure 2. a) Polarization curves for blank CF, Cu_3P NW/CF, and Cu_3P MP/CF in 0.5 M H_2SO_4 with a scan rate of 2 $mV s^{-1}$. b) Tafel plots for Cu_3P NW/CF, Cu_3P MP/CF, and Pt/C.

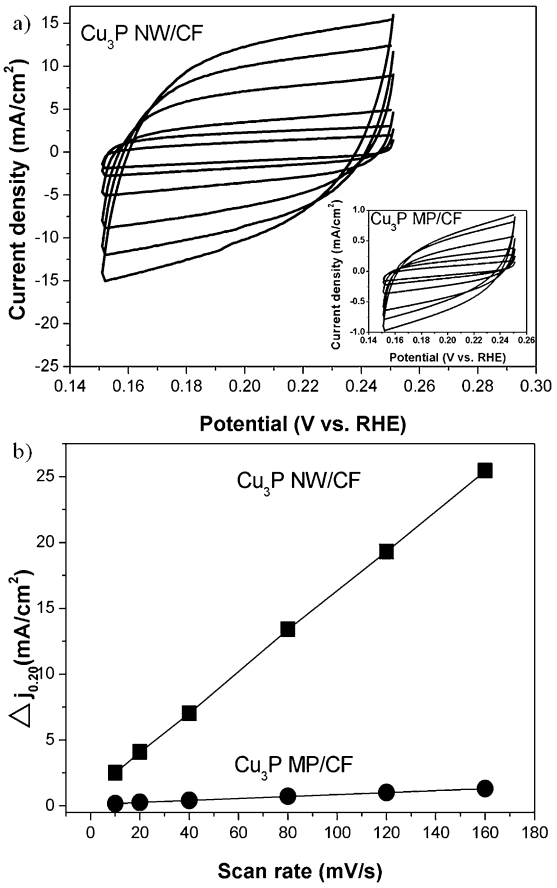

Figure 3. a) CVs for Cu_3P NW/CF and Cu_3P MP/CF (inset). b) The capacitive currents at 0.20 V as a function of scan rate for Cu_3P NW/CF and Cu_3P MP/CF ($\Delta j_0 = j_a - j_c$).

0.15–0.25 V, where the current response should only be due to the charging of the double layer (Figure 3). The capacitance of Cu_3P NW/CF and Cu_3P MP/CF is 77.8 and 4.1 $mF cm^{-2}$, respectively, thus indicating Cu_3P NW/CF has a much higher surface roughness than Cu_3P MP/CF. Thus, the large exchange current density of Cu_3P NW/CF can be associated with its high surface area.[22]

We also examined the durability of Cu_3P NW/CF. As shown in Figure 4, after continuous CV scanning for 3000 cycles in 0.5 M H_2SO_4 at a scan rate of 100 $mV s^{-1}$, the polarization curve shows negligible difference compared with the initial one. The inset of Figure 4 shows the time-dependent current density curve for Cu_3P NW/CF under a static overpotential of 200 mV. After a long period (25 h), the current density only shows slight degradation, which could be due to the consumption of proton in the system and the hindrance of the reaction by hydrogen bubbles remaining on Cu_3P NW/CF. Thus, this 3D electrode has superior stability in the long-term electrochemical process compared to defect-rich ultrathin MoS_2 nanosheets,[6d] amorphous MoS_2,[6f,g] and Ni_2P nanoparticles.[10a]

The superior catalytic performance and stability of the Cu_3P NW/CF cathode could be attributed to the following: 1) the direct integration of Cu_3P NWs onto CF enables good mechanical adhesion and electrical connection between them; 2) the good intrinsic electrical conductivity of Cu_3P[7] favors fast electron transport along the nanowire; 3) the nanowire array format not only allows fast vectorial electron transport,[12] but increases catalyst loading, thus leading to improved catalytic efficiency;[23] 4) the nanoscale dimension

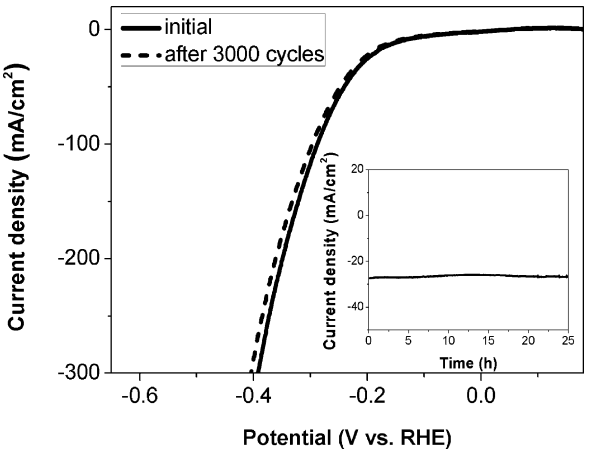

Figure 4. Polarization curves of Cu_3P NW/CF in 0.5 M H_2SO_4 initially and after 3000 CV scanning between +0.1 and −0.3 V vs. RHE. Inset: time-dependent current density curve for Cu_3P NW/CF under static overpotential of 200 mV for 25 h.

and high aspect ratio of Cu_3P NWs maximizes the number of exposed active sites and improves catalytic activity per geometric area;[13] 5) its 3D porous configuration allows easy diffusion of the electrolyte and thus more efficient utilization of active sites in Cu_3P.[24] Besides, the self-supported nature of Cu_3P NW/CF also avoids the use of polymer binder.

The generated gas was confirmed by gas chromatography (GC) analysis and measured quantitatively using a calibrated pressure sensor to monitor the pressure change in the cathode compartment of a H-type electrolytic cell. Potentiostatic cathodic electrolysis was performed by maintaining Cu_3P NW/CF at an overpotential of 200 mV for 90 minutes. By comparing the amount of measured hydrogen with calculated hydrogen (assuming 100% FE), we observe a FE close to 100% for the hydrogen evolution (see Figure S5 in the Supporting Information).

Figures S6a and S6b in the Supporting Information show the X-ray photoelectron spectroscopy (XPS) data for the 2p spectra in the Cu($2p_{3/2}$) and P(2p) regions for Cu_3P nanowires. One peak is apparent at 932.9 eV in the Cu($2p_{3/2}$) region, along with two peaks at 129.5 and 134.0 eV in the P(2p) region. The peaks at 932.9 and 129.5 eV are close to the binding energies for Cu and P in Cu_3P, and the peak at 134.0 eV for P can be assigned to oxidized P species arising from superficial oxidation of Cu_3P as a result of air contact.[25] The survey spectrum (Figure S6c) confirms the existence of oxygen in the sample. The Cu $2p_{3/2}$ binding energy of 932.9 eV is positively shifted from that of metallic Cu (932.6 eV; see Figure S7a in the Supporting Information) while the P 2p has a lower binding energy (129.5 eV) than red P (130.0 eV; Figure S7b).[25,26] It suggests that the Cu has a partial positive charge (δ^+) but the P has a partial negative charge (δ^-), thus implying transfer of electron density from Cu to P.[27] A metal complex HER catalyst incorporates proton relays from pendant acid-base groups, positioned close to the metal center where hydrogen evolution occurs,[28] and the active sites for hydrogenase also feature pendant bases proximate to the metal centers.[29] Our recent work show CoP and MoP as highly active HER catalysts consist of the metal center (δ^+) and the pendant base P (δ^-) close to it.[10d,e,f] Given that Cu_3P is also rich with metal centers (Cu; δ^+) and pendant bases (P; δ^-) positioned close to it, it is believed that it adopts a catalytic mechanism similar to that of metal complex, hydrogenase, CoP and MoP catalysts for the HER. The Cu and basic P act as the hydride-acceptor and proton-acceptor center, respectively, thus facilitating the HER.[9c,10a] The P could also facilitate the formation of copper hydride for subsequent hydrogen evolution by electrochemical desorption.[30]

It is important to note that the phosphidation temperature has a heavy influence on the HER activities of the catalysts. Figure S8 in the Supporting Information shows the polarization curves for these catalysts in 0.5 M H_2SO_4 with a scan rate of 2 mV s^{-1}. To achieve a current density of 50 mA cm^{-2}, it needs overpotentials of 439 mV, 232, 313, and 504 mV for the catalyst obtained at 220, 250, 270, and 300 °C, respectively. Figures S9 and S10 in the Supporting Information show the XRD patterns and SEM images of the products. A lower temperature of 220 °C leads to incomplete phosphidation while complete topotactic conversion occurs upon annealing at 250 °C. Further increase of the annealing temperature also exclusively gives Cu_3P products. However, the Cu_3P nanowires start to undergo coalescence at 270 °C or even change into porous film of microparticles at 300 °C. Thus, both effective phosphidation of a $Cu(OH)_2$ precursor and successful construction of nanowire arrays are key for high HER activity.

In conclusion, self-supported Cu_3P nanowire arrays on porous CF has been derived successfully from topotactic low-temperature phosphidation of its $Cu(OH)_2$ NW/CF precursor for the first time. When used as an integrated 3D hydrogen-evolving cathode, the Cu_3P NW/CF showed excellent catalytic performance and durability in acidic aqueous solutions. The excellent electrical conductivity and low price for metallic Cu, and the facile and scale-up preparation process, along with its remarkable activity and long-term aqueous stability of this 3D cathode, offer promising features for potential use in technological devices. Although the Cu_3P NW/CF exhibits amazing catalytic performance, two major hurdles need to be overcome for it to compete with platinum, including long-term durability and further decrease of the overpotential. These two issues could be mitigated by designing Cu_3P-coated conductive nanowire arrays or developing ternary TMPs using other transition-metal elements as promoters.[6h]

Experimental Section

Materials: Sodium hypophosphite (NaH_2PO_2) and metallic Cu were purchased from Aladdin Ltd. (Shanghai, China). Sulphuric acid (H_2SO_4), hydrochloric acid (HCl), sodium hydroxide (NaOH), andAPS were bought from Beijing Chemical Corporation. Red phosphorus was purchased from Xilong Chemical Co., Ltd. CF with 2 mm in thickness was supplied by Changsha Liyuan New Material Co., Ltd. All the reagents were used as received. The water used throughout all experiments was purified through a Millipore system.

Synthesis of $Cu(OH)_2$ NW/CF: $Cu(OH)_2$ NW/CF was prepared according to reported method with minor modifications.[16] Typically, CF was firstly washed with HCl and water several times to remove the surface impurities. The cleaned CF (1 cm × 2 cm) was immediately immersed into a 15 mL aqueous solution containing 2 mmol APS and 40 mmol NaOH at room temperature for 30 min. Then the CF with precursor was washed with water several times and dried in air.

Synthesis of Cu_3P NW/CF: To prepare Cu_3P NW/CF, NaH_2PO_2 (0.02 g) was placed at the center of the tube furnace and $Cu(OH)_2$ NW/CF was placed at the downstream side of the furnace at carefully adjusted locations to set the temperature and the distance between them was measured to be about 21 cm. After flushed with Ar, the center of the furnace was elevated to 300 °C with a heating rate of 2 °C min^{-1} and held at this temperature for 60 min. The $Cu(OH)_2$ NWs/CF was kept at ~250 °C. After naturally cooled to room temperature under Ar, the loading for Cu_3P on CF was determined to be 15.2 mg cm^{-2} with the use of a high precision microbalance.

Characterizations: Powder XRD data were acquired on a RigakuD/MAX 2550 diffractometer with $Cu_{K\alpha}$ radiation ($\lambda = 1.5418$ Å). SEM measurements were carried out on a XL30 ESEM FEG scanning electron microscope at an accelerating voltage of 20 kV. TEM measurements were performed on a HITACHI H-8100 electron microscopy (Hitachi, Tokyo, Japan) with an accelerating voltage of 200 kV. XPS measurements were performed on an ESCALABMK II X-ray photoelectron spectrometer using Mg as the exciting source. GC analysis was carried out on GC-2014C (Shimadzu Co.) with

thermal conductivity detector and nitrogen carrier gas. Pressure data during electrolysis were recorded using a CEM DT-8890 Differential Air Pressure Gauge Manometer Data Logger Meter Tester with a sampling interval of 1 point per second.

Electrochemical measurements: All the electrochemical measurements were conducted in a typical three-electrode setup with an electrolyte solution of 0.5 M H_2SO_4 using Cu_3P NW/CF as the working electrode, a graphite plate as the counter electrode and a saturated calomel electrode (SCE) as the reference electrode. In all measurements, the SCE reference electrode was calibrated with respect to reversible hydrogen electrode (RHE). Linear sweep voltammetry (LSV) measurements were conducted in 0.5 M H_2SO_4 with scan rate of 2 mV s^{-1}. All the potentials reported in our work were vs. RHE. In 0.5 M H_2SO_4, E (RHE) = E (SCE) + 0.281 V.

Received: March 31, 2014
Revised: May 22, 2014
Published online: July 15, 2014

Keywords: copper · electrochemistry · heterogeneous catalysts · hydrogen · nanostructures

[1] D. A. J. Rand, R. M. Dell, *Hydrogen Energy: Challenges and Prospects*, RSC, Cambridge, **2007**.
[2] a) M. G. Walter, E. L. Warren, J. R. McKone, S. W. Boettcher, Q. Mi, E. A. Santori, N. S. Lewis, *Chem. Rev.* **2010**, *110*, 6446; b) D. Merki, X. Hu, *Energy Environ. Sci.* **2011**, *4*, 3878.
[3] http://minerals.usgs.gov/minerals/pubs/mcs/2011/mcs2011.pdf.
[4] a) G. A. Le, V. Artero, B. Jousselme, P. D. Tran, N. Guillet, R. Métayé, A. Fihri, S. Palacin, M. Fontecave, *Science* **2009**, *326*, 1384; b) M. Hambourger, M. Gervaldo, D. Svedruzic, P. W. King, D. Gust, M. Ghirardi, A. L. Moore, T. A. Moore, *J. Am. Chem. Soc.* **2008**, *130*, 2015.
[5] a) D. E. Brown, M. N. Mahmood, M. C. M. Man, A. K. Turner, *Electrochim. Acta* **1984**, *29*, 1551; b) I. A. Raj, K. I. Vasu, *J. Appl. Electrochem.* **1990**, *20*, 32.
[6] For example, see: a) T. F. Jaramillo, K. P. Jørgensen, J. Bonde, J. H. Nielsen, S. Horch, I. Chorkendorff, *Science* **2007**, *317*, 100; b) J. Kibsgaard, Z. Chen, B. N. Reinecke, T. F. Jaramillo, *Nat. Mater.* **2012**, *11*, 963; c) M. A. Lukowski, A. S. Daniel, F. Meng, A. Forticaux, L. Li, S. Jin, *J. Am. Chem. Soc.* **2013**, *135*, 10274; d) J. Xie, H. Zhang, S. Li, R. Wang, X. Sun, M. Zhou, J. Zhou, X. Lou, Y. Xie, *Adv. Mater.* **2013**, *25*, 5807; e) Y. Li, H. Wang, L. Xie, Y. Liang, G. Hong, H. Dai, *J. Am. Chem. Soc.* **2011**, *133*, 7296; f) J. D. Benck, Z. Chen, L. Y. Kuritzky, A. J. Forman, T. F. Jaramillo, *ACS Catal.* **2012**, *2*, 1916; g) A. B. Laursen, P. C. K. Vesborg, I. Chorkendorff, *Chem. Commun.* **2013**, *49*, 4965; h) D. Merki, H. Vrubel, L. Rovelli, S. Fierro, X. Hu, *Chem. Sci.* **2012**, *3*, 2515; i) D. Kong, H. Wang, J. J. Cha, M. Pasta, K. J. Koski, J. Yao, Y. Cui, *Nano Lett.* **2013**, *13*, 1341; j) H. Vrubel, X. Hu, *Angew. Chem.* **2012**, *124*, 12875; *Angew. Chem. Int. Ed.* **2012**, *51*, 12703; k) W. Chen, K. Sasaki, C. Ma, A. I. Frenkel, N. Marinkovic, J. T. Muckerman, Y. Zhu, R. R. Adzic, *Angew. Chem.* **2012**, *124*, 6235; *Angew. Chem. Int. Ed.* **2012**, *51*, 6131; l) B. Cao, G. M. Veith, J. C. Neuefeind, R. R. Adzic, P. G. Khalifah, *J. Am. Chem. Soc.* **2013**, *135*, 19186; m) D. Voiry, H. Yamaguchi, J. Li, R. Silva, D. C. B. Alves, T. Fujita, M. Chen, T. Asefa, V. B. Shenoy, G. Eda, M. Chhowalla, *Nat. Mater.* **2013**, *12*, 850; n) J. Yang, D. Voiry, S. J. Ahn, D. Kang, A. Y. Kim, M. Chhowalla, H. S. Shin, *Angew. Chem.* **2013**, *125*, 13996; *Angew. Chem. Int. Ed.* **2013**, *52*, 13751; o) Y. Zhao, K. Kamiya, K. Hashimoto, S. Nakanishi, *Angew. Chem.* **2013**, *125*, 13883; *Angew. Chem. Int. Ed.* **2013**, *52*, 13638; p) J. Lin, Z. Peng, G. Wang, D. Zakhidov, E. Larios, M. J. Yacaman, J. M. Tour, *Adv. Energy Mater.* **2014**, DOI: 10.1002/aenm.201301875.
[7] S. T. Oyama, T. Gott, H. Zhao, Y.-K. Lee, *Catal. Today* **2009**, *143*, 94.
[8] a) S. Carenco, D. Portehault, C. Boissière, N. Mèzailles, C. Sanchez, *Chem. Rev.* **2013**, *113*, 7981; b) R. Prins, M. E. Bussell, *Catal. Lett.* **2012**, *142*, 1413.
[9] a) J. O. M. Bockris, E. C. Potter, *J. Electrochem. Soc.* **1952**, *99*, 169; b) P. Liu, J. A. Rodriguez, T. Asakura, J. Gomes, K. Nakamura, *J. Phys. Chem. B* **2005**, *109*, 4575; c) P. Liu, J. A. Rodriguez, *J. Am. Chem. Soc.* **2005**, *127*, 14871.
[10] a) E. J. Popczun, J. R. McKone, C. G. Read, A. J. Biacchi, A. M. Wiltrout, N. S. Lewis, R. E. Schaak, *J. Am. Chem. Soc.* **2013**, *135*, 9267; b) Y. Xu, R. Wu, J. Zhang, Y. Shi, B. Zhang, *Chem. Commun.* **2013**, *49*, 6656; c) E. J. Popczun, C. G. Read, C. W. Roske, N. S. Lewis, R. E. Schaak, *Angew. Chem.* **2014**, *126*, 5531; *Angew. Chem. Int. Ed.* **2014**, *53*, 5427; d) Q. Liu, J. Tian, W. Cui, P. Jiang, N. Cheng, A. M. Asiri, X. Sun, *Angew. Chem.* **2014**, *126*, 6828; *Angew. Chem. Int. Ed.* **2014**, *53*, 6710; e) J. Tian, Q. Liu, A. M. Asiri, X. Sun, *J. Am. Chem. Soc.* **2014**, *136*, 7587; f) Z. Xing, Q. Liu, A. M. Asiri, X. Sun, *Adv. Mater.* DOI: 10.1002/adma.201401692.
[11] J. D. Roy-Mayhew, G. Boschloo, A. Hagfeldt, I. A. Aksay, *ACS Appl. Mater. Interfaces* **2012**, *4*, 2794.
[12] J. Liao, D. Higgins, G. Lui, V. Chabot, X. Xiao, Z. Chen, *Nano Lett.* **2013**, *13*, 5467.
[13] Z. Chen, D. Cummins, B. N. Reinecke, E. Clark, M. K. Sunkara, T. F. Jaramillo, *Nano Lett.* **2011**, *11*, 4168.
[14] Y. Shuang, X. Huang, D. Ma, H. Wang, F. Meng, X. Zhang, *Adv. Mater.* **2014**, *26*, 2273.
[15] L. De Trizio, A. Figuerola, L. Manna, A. Genovese, C. George, R. Brescia, Z. Saghi, R. Simonutti, M. Van Huis, A. Falqui, *ACS Nano* **2012**, *6*, 32.
[16] H. Hou, Y. Xie, Q. Li, *Cryst. Growth Des.* **2005**, *5*, 201.
[17] Q. Guan, W. Li, *J. Catal.* **2010**, *271*, 413.
[18] A. E. Henkes, Y. Vasquez, R. E. Schaak, *J. Am. Chem. Soc.* **2007**, *129*, 1896.
[19] a) B. E. Conway, B. V. Tilak, *Electrochim. Acta* **2002**, *47*, 3571; b) N. Pentland, J. O. M. Bockris, E. Sheldon, *J. Electrochem. Soc.* **1957**, *104*, 182.
[20] C. C. L. McCrory, S. Jung, J. C. Peters, T. F. Jaramillo, *J. Am. Chem. Soc.* **2013**, *135*, 16977.
[21] S. Trasatti, O. A. Petrii, *J. Electroanal. Chem.* **1992**, *327*, 353.
[22] D. Kong, H. Wang, Z. Lu, Y. Cui, *J. Am. Chem. Soc.* **2014**, *136*, 4897.
[23] W. Zhou, X.-J. Wu, X. Cao, X. Huang, C. Tan, J. Tian, H. Liu, J. Wang, H. Zhang, *Energy Environ. Sci.* **2013**, *6*, 2921.
[24] S. H. Joo, S. J. Choi, I. Oh, J. Kwak, Z. Liu, O. Terasaki, R. Ryoo, *Nature* **2001**, *412*, 169.
[25] H. Pfeiffer, F. Tancret, T. Brousse, *Electrochim. Acta* **2005**, *50*, 4763.
[26] a) W. Kautek, J. G. Gordon, *J. Electrochem. Soc.* **1990**, *137*, 2672; b) *Practical Surface Analysis by Auger and X-ray Photoelectron Spectroscopy* (Eds.: D. Briggs, M. P. Seah), Wiley, New York, **1983**.
[27] *Encyclopedia of Inorganic Chemistry*, *2nd ed.* (Ed.: R. B. King), Wiley, Hoboken, **2005**.
[28] a) A. D. Wilson, R. H. Newell, M. J. McNevin, J. T. Muckerman, M. R. Dubois, D. L. Dubois, *J. Am. Chem. Soc.* **2006**, *128*, 358; b) A. D. Wilson, R. K. Shoemaker, A. Miedaner, J. T. Muckerman, D. L. Dubois, M. R. Dubois, *Proc. Natl. Acad. Sci. USA* **2007**, *104*, 6951; c) B. E. Barton, T. B. Rauchfuss, *J. Am. Chem. Soc.* **2010**, *132*, 14877.
[29] Y. Nicolet, A. L. de Lacey, X. Vérnede, V. M. Fernandez, E. C. Hatchikian, J. C. Fontecilla-Camps, *J. Am. Chem. Soc.* **2001**, *123*, 1596.
[30] W. Zhang, J. Hong, J. Zheng, Z. Huang, J. Zhou, R. Xu, *J. Am. Chem. Soc.* **2011**, *133*, 20680.

